Plasmonics (2020) 15:1977–1988
https://doi.org/10.1007/s11468-020-01178-8

Effect of Symmetry Breaking on Plasmonic Coupling in Nanoring Dimers

Bereket Dalga Dana[1] · Alemayehu Nana Koya[2] · Xiaowei Song[1] · Jingquan Lin[1]

Received: 2 September 2019 / Accepted: 4 May 2020 / Published online: 4 July 2020

Abstract
Breaking the morphological and compositional symmetries of metallic nanoparticle (NP) dimers provides a novel approach to modulate plasmon coupling between the NPs. In this study, we theoretically investigate the effect of symmetry breaking on the plasmonic coupling in morphologically asymmetric Au nanoring-nanodisk (NR-ND) dimer, compositionally heterogeneous Au-Ag nanoring dimer, and compositionally as well as morphologically asymmetric Au-Ag NR-ND heterodimers. It has been found that when the inner radii of symmetrical Au NR dimer is decreased, the scattering spectral intensity of coupled bonding mode and higher-order coupled bonding mode drastically decreases and increases, respectively. Besides, the effect of aspect ratio on the plasmon resonance modes is investigated. Furthermore, with fixed geometric parameters of one NR and by morphing the shape of the other NR into ND through inner radius, we show the generation and modification of a Fano resonance. As a result of introducing morphological and compositional asymmetry separately, single Fano-type spectral feature is observed in the scattering spectra. We demonstrate that the double Fano resonances can be easily achieved in compositionally and morphologically asymmetric heterodimer with double symmetry breaking. These dual modes are caused by the interference of dipolar bright mode (localized LSPR modes) of Ag NP with the quadrupole and hexapole modes (interband transitions) of the Au NP. Finally, at optimum asymmetric heterodimers, we discussed the effect of refractive index on the Fano-type resonance. These new and simple designs provide a novel insight to modulate optical response and the generation of higher-order Fano resonances, which have many potential applications such as in photonics and refractive index sensing.

Keywords Plasmon coupling · Symmetry breaking · Fano resonances · Refractive index sensing

Introduction

Localized surface plasmon resonance (LSPR) arises in the noble metal nanostructures due to the collective oscillation of conduction band electrons in response to external electromagnetic field [1, 2]. These resonance properties are highly dependent on the shape, size, material composition, and the refractive index of the surrounding medium of the nanostructures [3–5]. Moreover, it has attracted extensive research interest because of many promising applications in areas such as chemical and biological sensing [6], negative index materials [7], plasmonic waveguiding [8, 9], and information technology [1]. Apart from numerous LSPR modes due to different shapes of single nanoparticles (NPs), hybridization of these modes in strongly coupled metallic nanostructures at various alignments through electrostatic forces also enhances optical properties of plasmonic nanoparticles and their application [10, 11]. An in-phase mode in symmetrical dimers is optically bright, whereas the out-of-phase mode is dark due to the cancelation of the equivalent dipole moments [12]. On the other hand, in asymmetric heterodimers, out-of-phase modes can be excited with a plane wave which makes these systems very interesting for sensing applications [13]. Thus, due to its broken symmetry, asymmetric heterodimers are expected to support both dipolar and dark plasmon modes at the same time [12] as well as play a key role in the generation of additional plasmonic modes (or Fano-like resonances) [14].

Effect of symmetry breaking in different nanostructures is an important technique in the field of plasmonics [15, 16]. Symmetry breaking is a systematic and efficient way to

✉ Xiaowei Song
songxiaowei@cust.edu.cn

✉ Jingquan Lin
linjingquan@cust.edu.cn

[1] School of Science, Changchun University of Science and Technology, Changchun 130022, China

[2] Istituto Italiano di Tecnologia, via Morego 30, 16163 Genoa, Italy

modulate the optical property purposefully and possess a wide range of applications [10] as well as it introduces effects that are not present in the symmetrical plasmonic system [17, 18]. Moreover, it can be obtained by designing heterodimers consisting nanostructures of different shapes and sizes [19–21], various composition [13, 18, 22, 23], and different morphology as well as composition [12, 24]. Broken symmetry in nonconcentric ring/disk cavities [25, 26], asymmetric Au NP heterodimers [19], and simple structures, such as metallic nanodisks with a missing wedge-shaped slice [27], can support Fano-like resonances. These resonances are typically more sensitive to shapes of the nanoparticles and changes of the refractive index of the environment [28]. Wu et al. have also demonstrated the effect of broken symmetry on the plasmon coupling in the gold nanotube dimer and observed strong Fano-like resonance in the scattering spectrum [29]. This resonance usually emerges from the hybridization of the bright and the dark modes of radiative electromagnetic waves [28]. On the other hand, compositionally asymmetric Au-Ag NP heterodimers are extensively sought for applications in photonics, sensing, and catalysis [30]. Moreover, these asymmetric heterodimers introduce significant impacts on the optical responses of plasmonic nanoparticle dimers [13]. It has been anticipated that in compositionally asymmetric heterodimers consisting of two different materials [31], the couplings between surface plasmon resonance of the Ag NP and the continuum of interband transitions of the Au NP have also been investigated, and Fano resonances have been observed. Moreover, introducing morphological and compositional asymmetry is another way of producing Fano resonances and introduces intense impacts on the optical responses of plasmonic nanoparticle dimers.

Previously, most studies focused on the coupling behavior of plasmonic resonance modes for isometric and symmetrical NP homodimers, e.g., nanorings [32–34], nanodisks [32, 35, 36], and nanocubes [37, 38]. In these plasmonic systems, the LSPR of individual nanoparticles was used to enhance the optical response of the coupled system but does not play any role in the appearance of the Fano resonances. Meanwhile, recent reports have pointed out that further coupling of asymmetric morphologies of Ag NPs and compositionally asymmetry of Au-Ag heterodimers consisting of different morphologies and compositions can provide a novel way to modulate optical properties [10, 13]. Unlike symmetric dimer, these asymmetric heterodimers can lead to the manifestation of Fano resonance [31, 39]. It has been received considerable attention due to their potential applications in chemical and biological sensors, near-field imaging, optical waveguides, and nonlinear optical devices [7, 40]. Fano resonance has also been reported theoretically and experimentally to a lesser extent in morphological and compositionally asymmetric heterodimers [19, 41, 42]. Besides, nanorings are versatile structures that give several degrees of freedom to change their shape into other nanostructures [43]. More specifically, by modulating their inner radii and width, one can readily morph nanoring dimer into nanodisk dimer which enables control and manipulation of the optical responses of nanostructures for morphology-based applications [44]. Therefore, the interaction between asymmetric heterodimers is not as completely understood as in the homodimer. However, there has been a lack of detailed study on the effect of symmetry breaking on the optical responses of the nanoring-nanodisk system, by morphing the shape of other nanoring into nanodisk through the inner radius and the dimer width. Nevertheless, to the best knowledge of the authors, modulating the optical responses of nanorings dimer by morphing, its constituent nanostructures into nanodisks as functions of nanostructure size and width have not yet been reported. Moreover, the effect of morphological and compositional symmetry breaking on the optical response of plasmonic nanodimers is yet to be clarified. Therefore, a theoretical investigation on the plasmon coupling modes arising from asymmetric morphologies and composition of NP heterodimers is desired.

In this paper, we study the optical responses of various designs of plasmonic nanodimers by breaking morphological and compositional symmetries of the comprising nanostructures using computational finite-difference time-domain (FDTD) method. By controlling the inner radii and width of symmetrical Au NR dimer, we systematically investigate its optical response by morphing the constituent nanorings (NRs) into nanodisks (NDs). Also, the effect of aspect ratio on plasmonic properties of symmetric Au NR dimers is investigated. Particularly, by morphing the shape of one Au NR into ND through the inner radius and width, we show the generation and modification of a single Fano resonance in asymmetric Au NR-ND heterodimer. Besides, the effect of symmetry breaking on the optical response of compositionally asymmetric Au-Ag NR dimer is discussed. To further investigate the effect of symmetry breaking, we construct compositionally and morphologically asymmetric heterodimer comprised of Au nanoring and Ag nanodisk. Moreover, morphological and compositional asymmetric heterodimers can effectively generate higher-order Fano resonances and controls its resonant wavelength. Lastly, the potential for the use of the Fano resonances of asymmetric Au NR-ND and Au-Ag NR-ND heterodimers for sensing applications was evaluated.

Models and Methods

A schematic illustration of the studied nanostructures (Au NR dimer, asymmetric Au NR-ND, compositionally heterogeneous Au-Ag NR, and compositionally as well as morphological asymmetric Au-Ag NR-ND dimers) is shown in Fig. 1.

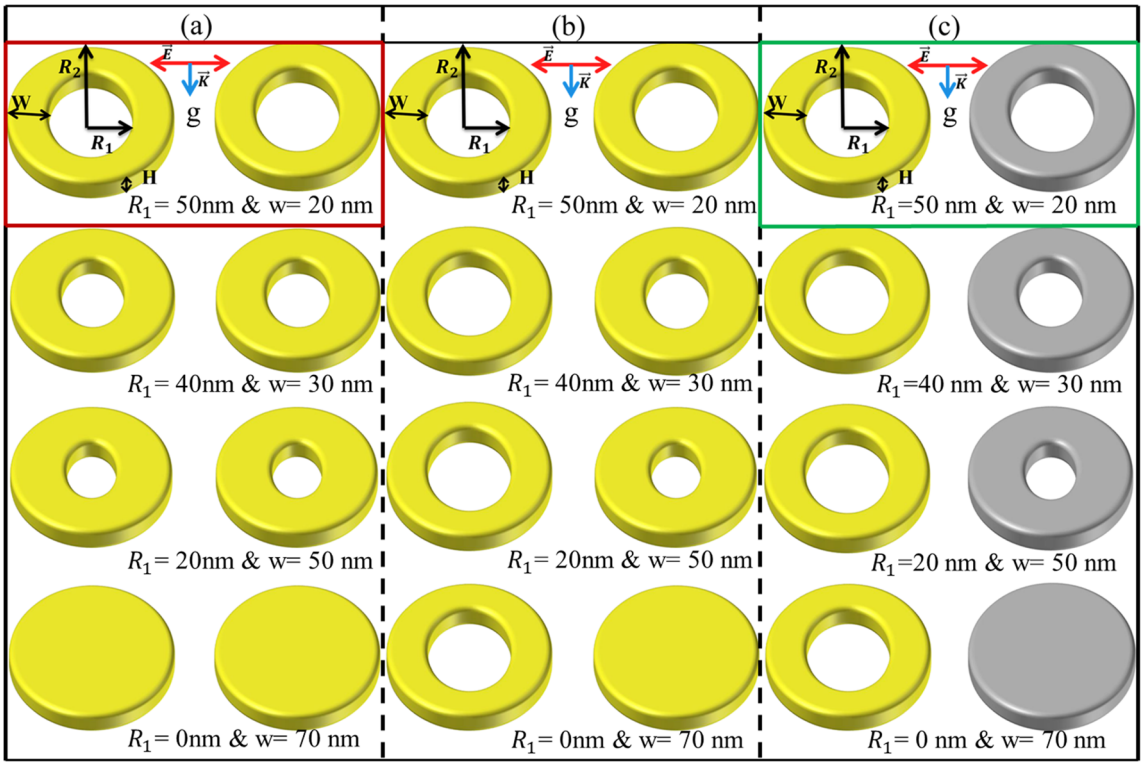

Fig. 1 **a** Shows the geometric description of the constantly morphed process from symmetrical Au nanoring dimer (top) into Au nanodisk homodimer (bottom) through inner radii and dimer width. **b** Illustrates the geometric depiction of constantly morphed process from Au nanoring homodimer (top) into morphologically asymmetric Au nanoring-nanodisk dimer (bottom) as a function of the inner radius of one nanoring. **c** Exhibits geometric illustration of the constantly morphed process from compositionally heterogeneous Au-Ag nanoring dimer (top green rectangular box) into compositionally as well as morphological Au-Ag nanoring-nanodisk heterodimer (bottom) through the inner radius of Ag nanoring. The dimer gap is shown by g. The outer radii and the thickness (height) of the nanorings were set to be $R_2 = 70$ nm and H = 50 nm, respectively. The arrows in the inset **a**, **b**, and **c** illustrate the directions of the polarization (red) and wave vector (blue)

Initially, we used symmetrical Au NR dimers, which were kept at a gap of g = 20 nm and with equal height or thickness (H = 50 nm) and outer radii($R_2 = 70$ nm). Later, to explore the influence of morphing effect on the optical responses of symmetrical Au nanoring dimer, we change gradually the shape of Au nanoring dimer (top) into completely equivalent Au nanodisk homodimer (bottom) as shown in Fig. 1 a. Furthermore, to explore the effect of aspect ratio on the plasmon coupling behavior of symmetric Au nanoring dimers, the ratio of outer diameter to thickness is systematically varied from 1.5 to 2.8. Moreover, to investigate the effect of symmetry breaking on the optical responses, we constructed morphologically asymmetric Au NR-ND heterodimer by fixing the geometry of one NR and constantly morphing the shape of the other NR into ND by changing its inner radius from 50 to 0 nm as shown in Fig. 1 b from the top to bottom. And also, we engineered compositionally heterogeneous Au-Ag nanoring dimer to investigate the effects of symmetry breaking on plasmon coupling (see the top green rectangular box in Fig. 1c). To further investigate the effect of symmetry breaking, we constructed compositional and morphologically asymmetric heterodimer by fixing the shape of gold nanoring and constantly changing the shape of silver nanoring into nanodisk through inner radius as shown in Fig. 1 c. Finally, we investigate the applications of the Fano resonances in refractive index sensing. The optical responses of both symmetric and asymmetric dimer are interpreted from the perspectives of a plasmon hybridization model [45]. This analytical model has been applied to various asymmetric heterodimers such as a dual-disk ring structure [46], concentric semi-disk ring cavities [47], asymmetric split nanorings [48], and symmetric ring [49], and it has shown a good quantitative agreement with numerical approaches. It has been used to explore the coupling mechanism the Fano resonances in the morphologically and compositionally asymmetric heterodimers [50].

The symmetric dimer and asymmetric heterodimers were suspended in air and illuminated by a linearly polarized plane wave, which was injected along the z-axis, perpendicular to the plane of the nanostructures. Polarization of the incident light was aligned along the interparticle axis of the dimer (see the inset in Fig. 1). The optical responses of symmetrical dimer and asymmetrical heterodimers were simulated with the time-domain FDTD solutions. Scattering intensities of the studied nanostructures were calculated using total-field-scattered-field (TFSF) source that covers a spectral range from 300 to 1600 nm. The dielectric functions of

the studied materials were modeled using the experimental data of Johnson and Christy [51]for the gold and Palik [52] for silver. We used a perfectly matched layer (PML) boundary conditions to ensure total absorption of electromagnetic radiation at the simulation boundaries. Throughout the study, the mesh sizes used during the simulation were varied between 1 and 2 nm in all three dimensions. The convergence test of the calculation has been carried out, and the results presented in the present study shows that the error is within the acceptable level [53].

Results and Discussion

Effects of Morphing Nanoring into Nanodisk

Recently, it has been demonstrated that morphing nanostructures play significant roles in controlling optical responses for both single and coupled nanoparticles [10, 54]. Therefore, it is important to study the effects of such parameters on the far- and local-field responses of symmetrical NP dimers. Here, we explore the impact of inner radii(R_1) and the width (w) of the constituent nanorings on the optical responses of symmetrical Au nanoring dimer. For a fixed thickness, the outer radii, and the dimer gap of symmetric Au NR dimer, we decreased the inner radii from 50 to 0 nm and correspondingly increased the width of the constituent nanorings from 20 to 70 nm (see Fig. 1a). Figure 2(a) shows the scattering spectrum of Au nanoring dimer that is constantly morphed into nanodisk dimer by controlling inner radii and width. The scattering intensity of symmetrical Au nanoring dimer with $R_1 = 50$ nm and $w = 20$ nm in Fig. 2(a) red curve exhibits two well-defined peaks: a coupled bonding mode and high-order coupled bonding mode (hereafter, mode I and mode II, respectively) at 936 and 816 nm [32]. The mode I observed at 936 nm is due to the strong coupling between the local fields accumulated at the inner and outer walls of symmetric nanorings [34], and mode II observed at 816 nm is resulting from the weak coupling of the resonance modes of the two nanorings [55]. The scattering spectra of symmetric Au nanodisk dimer with ($R_1 = 0$ and $w =$ 70 nm) in Fig. 2(a) violet curve had only a single dominant dipole mode resulting from strong coupling is observed at

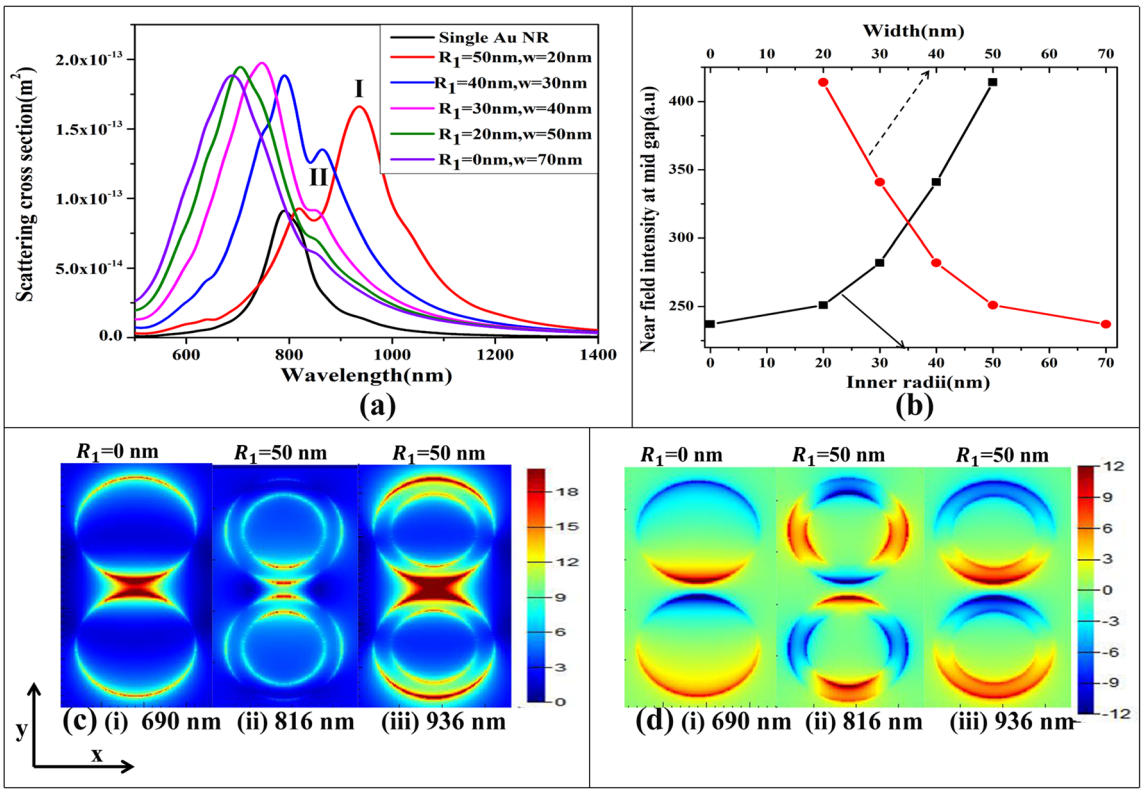

Fig. 2 Effect of morphing on the spectral responses and local electric-field amplitude of symmetric Au NR homodimer. **(a)** Represent scattering cross sections of monomer Au NR and scattering spectrum of morphing symmetrical Au NR into Au ND homodimer as a function of inner radii and dimer width of NRs with polarization along the dimer axis. **(b)** Quantitative representation of local electric field intensities of mode I at mid-gap of the dimer as a function of inner radii (black curve) and width (red curve). **(c)** and **(d)** Local-field and surface charge distribution profiles of Au NR and ND homodimers as a function of the inner radius of the constituent NRs, respectively. The outer radii and the thickness (height) of the Au nanoring homodimer were set to be $R_2 = 70$ *nm* and H = 50 *nm*, respectively, and the interparticle separation distance of the homodimer was fixed be g = 20 *nm*

690 nm. Hence, the effect of morphing nanoring into nanodisk dimer plays an important role in the coupling behavior of LSPR modes.

To further understand the contributions of individual LSPR in the symmetric Au nanoring dimer, we separately simulate the scattering spectra of a single Au nanoring, as shown in Fig. 2(a) black curve. The scattering spectrum of monomer Au nanoring is dominated by a single peak at 800 nm. The plasmon coupling behavior of this dimer leads to the red-shifting of the electromagnetic spectrum and shows the higher intensity of the electromagnetic spectrum [55]. These red-shifts of LSPR wavelength signatures the strong plasmon coupling in the case of Au nanoring dimer as compared to single Au nanoring.

The intensity of modes I and II in symmetric Au nanoring dimer is significantly affected by morphing process through the size of inner radii and width of the constituent nanorings. For fixed outer radii and the thickness, when symmetric Au nanoring dimer is gradually changed into Au nanodisk dimer by decreasing (increasing) the inner radii (the width), the scattering spectra of mode I peak lose intensity and become very weak. This is due to the disappearance of the local EM fields' distribution confined at the inner wall of nanorings [34, 56]. This can be further confirmed from their corresponding near-field intensity maps (see Fig. 2(c)). In contrast, due to raising the confinement of the local electric distributions at the outer walls of Au nanodisk dimer, mode II significantly gains intensity and finally becomes the dominant dipole mode in scattering spectra [57]. Besides, as one increases the width, the scattering intensity of mode II tends to increase in spectral width and exhibits a broader spectrum [34] (see Fig. 2(a) violet curve). Moreover, for the smallest inner radii, a strong dipole-dipole coupling mode of symmetric Au nanodisk dimer locates at 690 nm. It was found that when the inner radii (width) decreased (increased), the intensity of modes I and II considerably decreased and increased, respectively. These results indicate that the influence of the morphing effect in symmetric Au nanoring dimer shows the remarkable changes in the plasmon coupling modes in terms of intensity and peak positions.

To further investigate the underlying physics of these modes, we calculate the local EM field and the surface charge distribution profiles of the corresponding peaks. As can be seen from Fig. 2(c), the local EM field distribution is extremely affected by the morphing process through inner radii and the width. For mode I at ($R_1 = 50$ and $w = 20$ nm), the local electric field is confined at the midpoint of the Au nanoring homodimer as shown in Fig. 2(c)(iii). This field distribution profile is exactly caused by the symmetric coupling between the interior and the exterior surfaces of the dimer [58]. As shown in Fig. 2(d)(iii), this mode displays a dipole-dipole mode in the surface charge distributions. This indicates that mode I is an in-phase plasmonic coupling mode [18]. Unlike mode I, the local electric field intensity of mode II is weak, and the surface charge distribution exhibits a quadrupole-quadrupole pattern as shown in Fig. 2(c)(ii) and (d)(ii), respectively. The same edge of Au nanoring dimer shows the opposite signs. Furthermore, the local electric field distribution profiles of mode II in Au nanodisk dimer reveals that their distributions are mainly concentrated around the outer surface of Au nanodisks and a dipole-dipole mode in the surface charge pattern along the polarization direction as shown in Fig. 2(c)(i) and (d)(i), respectively.

The above facts supported by the electromagnetic near-field intensity of mode I calculated at the center of gap region of symmetric Au NR dimer as a function of the inner radii and width as shown in Fig. 2(b). Due to spatial overlap of the local EM field distributions, the near-field coupling strength of this mode is found to be stronger. However, as one decreases the inner radii from 50 to 0 nm, the near-field intensity of the mode I at the junction of the homodimer system decreases from 414 (a.u) to 237 (a.u) as shown in Fig. 2(b) black curve. To further support our results, as one increases the width from 20 to 70 nm, the near-field intensity of this mode decreases from 305 (a.u) to 249 (a.u) (see the inset shown in Fig. 2(b) red curve). It is note that, in both cases, the near-field intensity of this mode decreases through the inner radii (black curve) and width (red curve) of the constituent nanorings.

To quantify the blue-shift trend for the LSPR wavelengths of these modes with decreasing (increasing) the inner radii (width), the behaviors of the resonance wavelengths were discussed for these parameters. As one can decrease the inner radii, the resonance mode I and II found to blue-shift as shown in Fig. 2(a). This is due to the weak plasmonic coupling between charges at the outer and inner surfaces of symmetric nanorings. Moreover, increasing the width of nanoring results in an increase of the distance between the inner and outer walls of the nanoring and gives rise to a weak coupling of the localized plasmons excited at both walls [34], which is manifested by the blue-shift of modes I and II. It is seen that the response is spectrally blue-shifted for both modes, though the effect is more pronounced for mode II. It is revealed from Fig. 2(a) that the LSPR of modes I and II are blue-shifted as R_1 decreased and w increased simultaneously. The observed modification of these modes can be understood by the plasmon coupling between the inner and outer surfaces of symmetrical Au nanoring homodimer through inner radii and width.

In general, one can note two important observations about the spectral behavior of constantly morphing Au nanoring homodimer into Au nanodisk homodimer. First, as one decreases, the inner radii of symmetric Au nanoring homodimer, the scattering spectrum of mode I lose intensity, which can be ascribed to the disappearance of the local electric fields accumulated at the inner walls. In contrast, mode II drastically gains intensity due to the increased confinement of local-

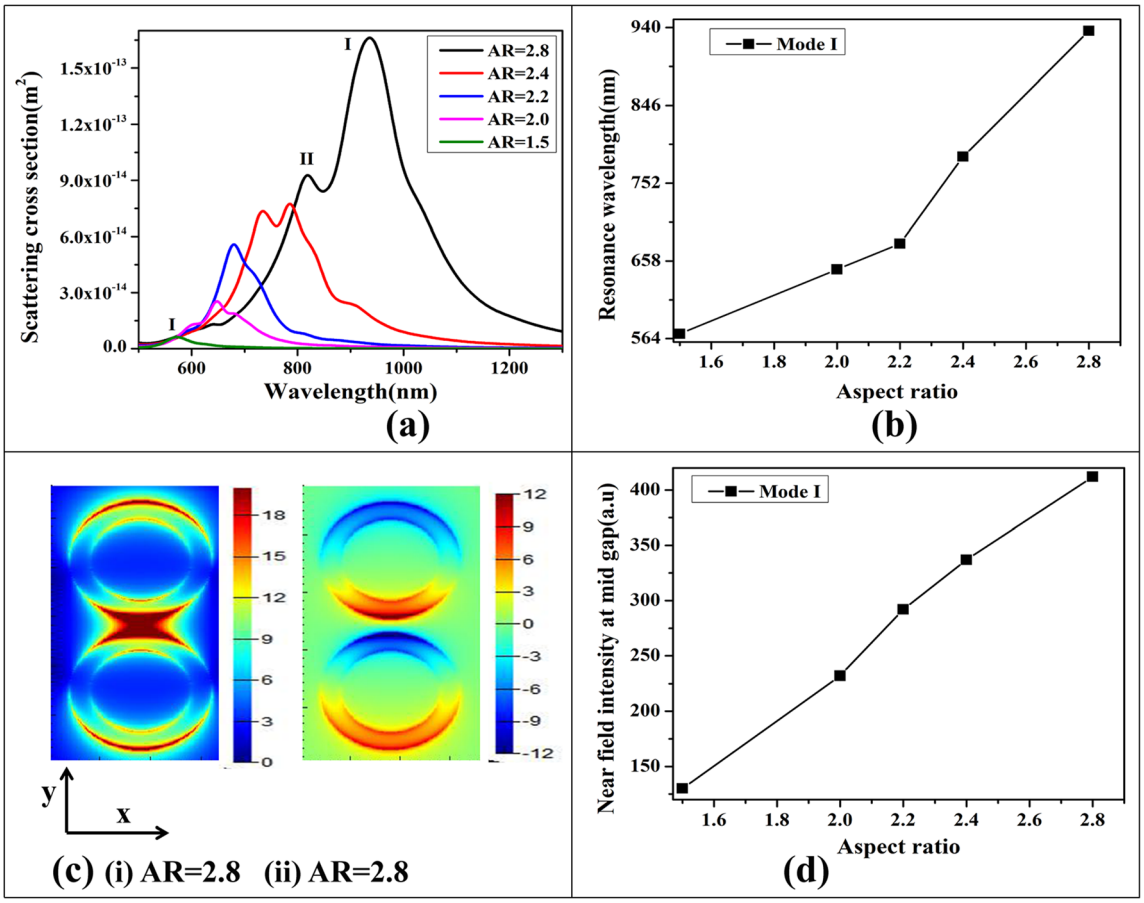

Fig. 3 Effect of aspect ratio on the plasmon resonance mode of symmetric Au nanoring dimer. (**a**) Calculated scattering spectra of gold nanoring dimers with varied aspect ratios under the polarization is along the dimer axis. (**b**) Represents resonance wavelengths of mode I as a function of aspect ratios. (**c**) (i and ii) Local electric field and surface charge distributions of Au nanoring homodimers with an aspect ratio of 2.8, respectively. (**d**) Quantitative representation of near-field intensities of mode I at mid-gap of the dimer as a function of aspect ratios

field distributions at the outer walls (or edges) of Au nanodisk homodimer. Second, the effect of morphing can also cause a blue-shift of resonance peak on these modes.

Effects of Aspect Ratio on the Plasmon Resonance Mode

Aspect ratio (diameter/thickness) is one of the applicable factors that allow controlling plasmon resonance of Au nanoring dimers [59]. To investigate the modulation of optical response with the aspect ratio, we represent the simulation results for the scattering spectra of symmetric dimer as shown in Fig. 3. We have altered the aspect ratio from 1.5 to 2.8 and obtained by varying the diameter and thickness of Au nanorings. Figure 3 (a) shows the effect of changing the aspect ratios of symmetric Au nanoring dimer. For a given symmetric Au nanoring dimer, the scattering spectra of this system with an aspect ratio (AR = 1.5) show only a single dominant coupled bonding mode (mode I) located at 570 nm with much smaller scattering intensity (see Fig. 3(a) green curve). It is revealed that there is a spectral red-shift as well as the increased spectral intensity of this mode with the increased aspect ratio [59]. Figure 3(b) shows that, with increasing the aspect ratio of Au nanoring dimer, the linear relationship of mode I is observed. This linear relationship between resonance wavelengths with aspect ratio provides an idea that the LSPR of the dimers can be altered from visible to the near-infrared region [60]. Hence, this mode is fundamentally controlled by the aspect ratio and therefore allowing a reasonable modification of its resonance wavelength [61]. Moreover, for greater aspect ratio, the induced high-order coupled bonding mode (mode II) is observed. A similar phenomenon was reported by Tsai et al. for single elliptical gold nanorings [59].

The local electric field and surface charge distributions of mode I in Au nanoring homodimer with the largest aspect ratio (AR = 2.8) are calculated, as shown in Fig. 3(c). The high aspect ratio produces an apparent near-field intensity located at the midpoint of Au nanoring dimer (see Fig. 3(c)(i)). This field distribution profile is exactly caused by the coupling between the interior and the exterior surface of Au nanorings. The charge distribution of this mode shows the same signs at the inner and outer surfaces of Au nanoring dimer, as shown in

Fig. 3(c)(ii). Also, we calculated near-field intensity of mode I at mid-gap of Au nanoring dimer with the different aspect ratio quantitatively, as shown in Fig. 3(c). As the aspect ratio is increased, the field intensity is significantly raised. As shown in the present study, increasing aspect ratio immensely affects the plasmon coupling behaviors of symmetric Au nanoring dimers. Moreover, it confirms that this near-field intensity with an aspect ratio of 2.8 is much stronger than with aspect ratio of 1.5.

Effects of Morphological Symmetry Breaking on Plasmon Coupling

Recent studies have pointed out that plasmon coupling modes of nanoparticles at different morphologies can provide the possibility to modulate optical responses due to broken symmetry [10]. To explore the effect of morphological symmetry breaking on the spectral behavior of plasmon coupling modes, we design asymmetrical Au nanoring-nanodisk heterodimer comprised of gold nanoring with fixed geometric parameters and the other nanoring constantly morphed into nanodisk (see Fig. 1(b)). The scattering spectrum of symmetrical Au nanoring dimer that is constantly morphed into asymmetric Au NR-ND dimer by fixing the geometry of the one NR and varying the inner radius of the other NR from 50 to 0 nm is displayed in Fig. 4(a). As we discussed in Effects of Morphing Nanoring into Nanodisk, the scattering spectra of Au NR homodimer with $R_1 = 50$ nm show two modes I and II at 936 and 816 nm, respectively (see Fig. 4(a) black curve). When the inner radius of nanoring decreases from 50 to 40 nm, the scattering spectra show three well-defined peaks mode I, II, and III at 909, 795, and 685 nm, respectively (see in Fig. 4(a) red curve). As we observed from Effects of Morphing Nanoring into Nanodisk, modes I and II are dipole-dipole and quadrupole-quadrupole resonance modes, respectively, whereas mode III is a hybrid mode and originates from the combination of dipole and quadrupole resonance modes [7]. Compared with symmetric Au nanoring dimer, this spectrum includes a new hybrid resonance mode that arises as a peak in the scattering spectra, which is recognized as a Fano resonance [14]. Moreover, the aforementioned modes are blue-shifted as the inner radius decreases to 0 nm. For example, the single Fano resonance appears at 580 nm for the cases of asymmetric Au NR-ND heterodimer (see Fig. 4(a) green curve). The generation of this Fano resonance is interpreted in terms of coupling of quadrupole and dipole modes [46]. We can observe that the effect of symmetry breaking through the inner radius of the second nanoring can effectively generate and control the resonant wavelength of the Fano resonance.

To identify the nature of Fano resonance, the local electric field and charge distribution profile of morphological asymmetric Au NR-ND heterodimer at 580 nm are simulated. As shown in Fig. 4(b)(i), the strong field distributions appears around the ND and displayed a dipole plasmon mode. It shows that the charge distribution of this mode revealed a dipole-quadrupole plasmon mode (see in Fig. 4(b)(ii)). It can be seen that the local electric field distribution profile becomes weak at the NR side and displayed a quadrupole mode (see the bottom NR in Fig. 4(b)(i) and (ii)). As we know, the interference between the bright and dark plasmonic modes can produce Fano resonance. Moreover, it can be seen from the local-field distribution of morphological asymmetric Au NR-ND heterodimer in Fig. 4(b)(i) that two hot spots exist in the ND (on the top) and four hot spots exist in the NR (on the bottom). The surface charge distribution profile as shown in Fig. 4(b)(ii) indicates that Fano resonance at 580 nm results from the coupling of bright dipole mode of ND and dark quadrupole mode of NR in morphological asymmetric Au

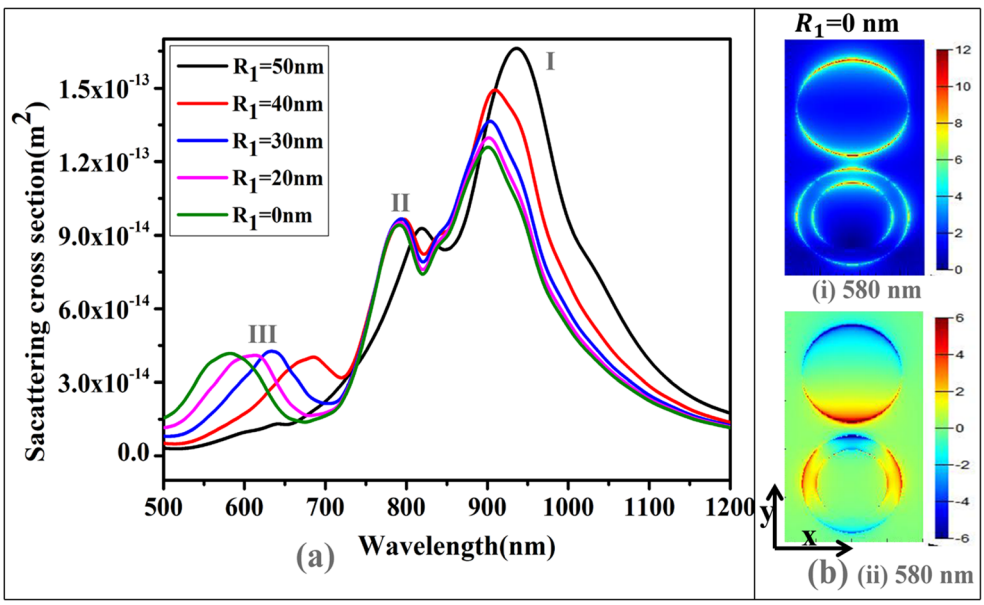

Fig. 4 Effects of morphological symmetry breaking on the spectral responses, local electric field and surface charge distribution of Au nanodimer. (a) The scattering spectra of asymmetrical heterodimers. (b) Represents locale electric-field and surface charge distribution profiles of asymmetrical Au NR-ND heterodimers for mode III at $R_1 = 0$

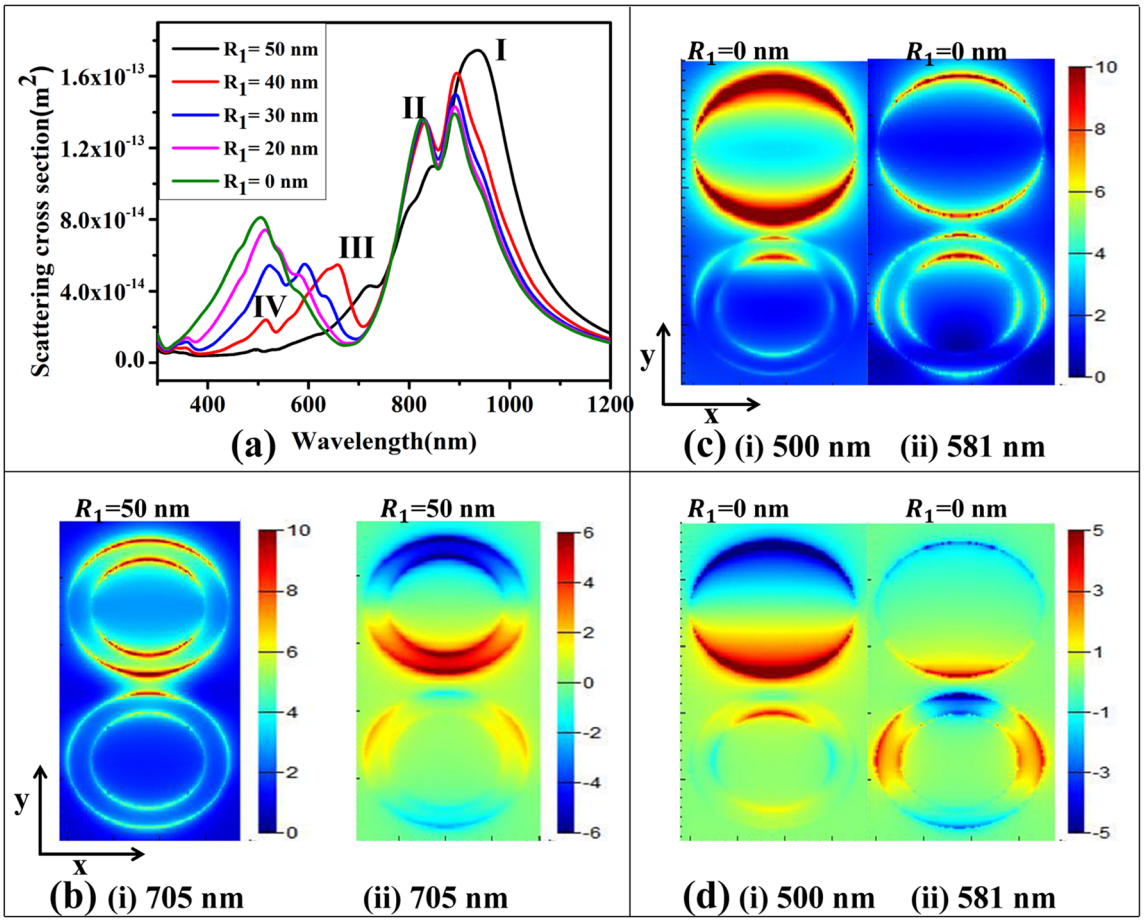

Fig. 5 Effects of morphological and compositional symmetric breaking on plasmon coupling in nanodimers. (a) The scattering spectra of compositional asymmetric and morphologically as well as compositionally asymmetric heterodimers. (b) The near-field and surface charge distribution profiles of mode III at 705 nm resonance mode with R_1 = 50 *nm*. (c) and (d) The near-field and surface charge distribution profiles of modes III and IV with R_1 = 0 nm

NR-ND heterodimer. Moreover, the above results evident that morphologically asymmetric heterodimers possess further spectral information in comparison with symmetric Au nanoring dimer.

Effects of Compositional Symmetry Breaking on Plasmonic Coupling

To demonstrate the effect of introducing compositional asymmetry on the plasmon coupling phenomenon, we separately calculate the scattering spectrum of a compositional heterodimer of $R_1 = 50$ *nm* composed of Au and Ag NRs suspended in the air as shown in Fig. 5(a). In compositionally asymmetric Au-Ag NR heterodimer (see the rectangular green box shown in Fig. 1(c)), scattering spectra show three peaks at 928 nm, 830 nm, and 705 nm, which are indicated by modes I, II, and III, respectively, as shown in Fig. 5(a) (black curve). The modes observed at 928 nm and 830 nm are due to the strong plasmon coupling between the inner and outer walls and the weak coupling between the resonances mode of the compositionally asymmetric Au-Ag NR heterodimer. This result clearly shows that the scattering spectra of modes I and II are due to the dipole LSPR of the Au and Ag NRs [22]. Compared to symmetric Au NR dimer in Fig. 2(a) (red curve), the scattering spectra shown in Fig. 5(a) black curve includes a new resonance mode (mode III) that appears at a given resonance wavelength, which is identified as a Fano resonance. This phenomenon arises from the coupling between the continuum of interband transitions in the Au NR and the discrete LSPR of the Ag NR, which can be observed from the surface charge distribution (see Fig. 5(b)(ii)). Further, we see that resonance wavelength of this Fano resonance is blue-shifted due to weak plasmon coupling of the constituent Au and Ag NR monomers compared with symmetric Au NR dimer. In addition to blue-shift, the intensity of the scattering spectrum of mode III is not that much strong because of the otherwise uncoupled plasmon modes of the asymmetrical heterodimer [13]. It clearly shows that introducing compositional asymmetry in symmetric dimer induces a Fano resonance.

In order to reveal further the origin of this Fano resonance, we investigate the surface charge and electric field distributions at the wavelength corresponding to mode III, which are

presented in Fig. 5(a) black curve. As for the mode III, the strong field distribution in Fig. 5(b)(i) is mainly concentrated around the Ag NR (on the top) and displayed a dipole plasmon mode. The weak field distributions on the Au NR (on the bottom) exhibit a quadrupole plasmon mode as shown in Fig. 5(b)(ii). Moreover, the electric field intensity is localized around the Ag NR of the Au-Ag NR heterodimer, and the surface charge distribution in the Ag NR exhibits a dipolar pattern, whereas the surface charge in the Au NR exhibits a quadrupolar pattern as shown in Fig. 5(b)(i) and (b)(ii), respectively. The quadrupolar charge pattern in the Au NR is induced by the electric field from the nearby Ag NR [18]. Hence, the coupling between compositionally asymmetric Au-Ag NR heterodimer and plasmon resonance modes is coupled differently due to the effect of symmetry breaking [13]. Due to reduced symmetry, the spherical harmonics are no longer orthogonal, and plasmons from the outer and inner surfaces of the NR dimer are no longer restricted to the same angular momentum [62]. This interaction leads to the possibility of generating the Fano resonance in the scattering spectra owing to a mixture of bright dipolar and dark quadrupolar plasmon modes.

We further broke the symmetry of compositional asymmetric Au-Ag NR heterodimer to generate higher-order Fano resonances. Introducing morphological and compositional asymmetry, we studied the optical response as the shape of Ag NP morphed from NR into ND through inner radius. The scattering spectrum of continuously morphing Au-Ag NR heterodimer into Au-Ag NR-ND heterodimer was calculated, with constantly varying the inner radius of Ag NR, from 50 to 0 nm as shown in Fig. 5(a). As we discussed above, compositionally asymmetric Au-Ag NR heterodimer shows three distinct resonance peaks at 928 nm, 830 nm, and 705 nm, and its optical response only supports a single Fano resonance mode around 705 nm (see Fig. 5(a) black curve). As one decreases the inner radius of the Ag NR from 50 to 40 nm, the scattering spectra exhibits four well-defined resonance modes, which are denoted by modes I, II, III, and IV at 895, 830, 659, and 516 nm, respectively, as shown in Fig. 5(a) red curve. Compared with compositionally asymmetric Au-Ag NR heterodimer with ($R_1 = 50$ nm), this spectra support two Fano resonance modes at 659 and 516 nm, which are known as higher-order Fano resonances. They are caused by the interference of dipolar bright mode of Ag NR (on the top) with the quadrupole and hexapole modes of Au NR (on the bottom) for modes III and IV, respectively. Moreover, the Fano resonance labeled at 516 nm is a new plasmonic resonance mode for Au-Ag NR heterodimer with ($R_1 = 40$ nm). The origin of this Fano resonance is a particularly interesting consequence of symmetry breaking due to heterogeneous in material and asymmetric in shape. As we have seen in Fig. 5(a), with a further decrease of the inner radius from 40 to 0 nm, modes III and IV are blue shifted about 78 nm and 16 nm, respectively. Specifically, a dramatic increase in intensity and broadening of the scattering spectra of mode IV can be observed. More interestingly, it can be seen that continuously morphing the inner radius of the Ag NR can effectively generate higher-order Fano resonances and control its resonant wavelength.

To further confirm the origin of higher-order Fano resonance modes III and IV, local electric field and surface charge distribution profiles of morphological and compositionally asymmetric Au-Ag NR-ND (R_1 *of Ag NR* $= 0$ *nm*) heterodimers were calculated, which provides a clear picture regarding the formation of the above Fano resonances (see Fig. 5(c) and (d)). The strong field distributions as shown in Fig. 5(c)(i) are mainly concentrated around the Ag ND (on the top), and the weak field distributions on the Au NR (on the bottom) exhibit four and six hot spots at the inner and the outer walls, respectively, which implied the existence of quadrupole and hexapole plasmon modes. The surface charge distribution in Fig. 5(d)(i) demonstrates that a dipolar mode of Ag NR or ND (on top) and the combination of quadrupole-hexapolar patterns of the Au NR (on bottom) are excited simultaneously. The quadrupolar-hexapolar charge pattern in the Au NR (on the bottom) is induced by the electric field from the nearby Ag NR or ND. It can be seen from the local-field distribution of Au-Ag NR-ND heterodimers in Fig. 5(c)(ii) that two hot spots exist in the ND and four hot spots exist in the Au NR. The surface charge distribution profile as shown in Fig. 5(d)(ii) indicates that higher-order Fano resonances at 581 nm result from the coupling between the dipole mode of Ag ND (on top) and the quadrupole modes of the Au NR (on bottom) structures in Au-Ag NR-ND heterodimers. It is found that introducing compositionally and geometrical asymmetry in Au-Ag NR-ND heterodimer can excite double Fano resonances.

Effect of Refractive Index on the Fano Resonances

Fano resonance is an interference resulting from the coupling of two or more excitation modes, thus intrinsically more sensitive to changes in geometry or environmental refractive index changes which can induce dramatic resonance shifts [7, 46]. The refractive index of the surrounding medium strongly affects the properties of Fano resonance (FR) [47]. The most interesting applications for the Fano resonances might be in refractive index sensing [63]. Surface plasmon resonance is sensitive to many factors, one of which is the refractive index of the surrounding medium [64]. Here, we discuss the effect of the refractive index on the Fano-type resonance of optimized asymmetric heterodimers. In this calculation, we used asymmetric Au-Ag NR-ND and Au-Ag NR-ND heterodimers: with the same outer radius ($R_2 = 60$ *nm*) and thicknesses (H = 50 *nm*) of the constituent NPs, whereas the inner radius/width (R_1/w) of NR and ND is 40 nm/20 nm and 0 nm/60 nm, respectively, to estimate the Fano resonance sensitivity

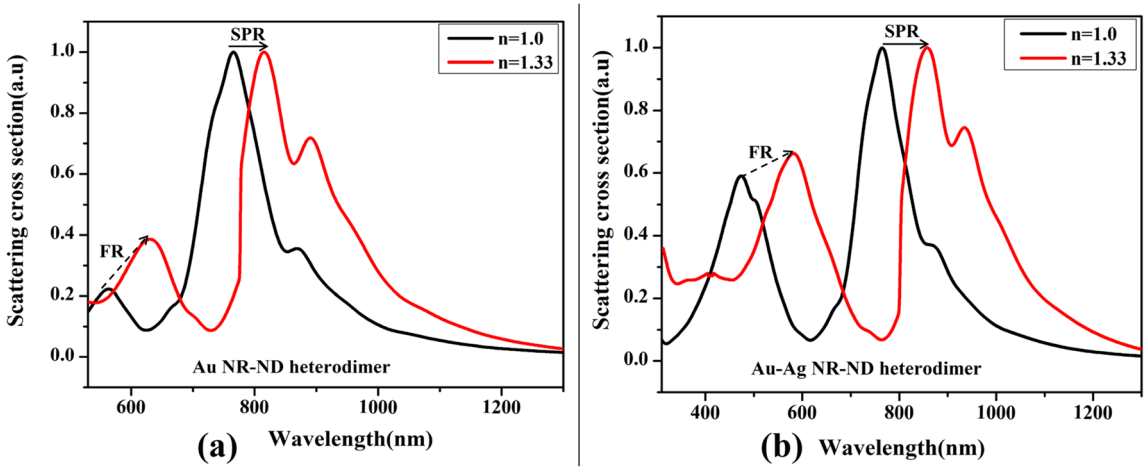

Fig. 6 The FR and SPR sensing in asymmetric heterodimers. **a** and **b** The scattering spectra of asymmetric Au NR-ND and Au-Ag NR-ND heterodimers with the different refractive index, respectively

to the refractive index change of the surrounding medium. The two NPs were kept at a gap of g = 20 *nm*. To calculate the sensitivity of asymmetric heterodimers to the surrounding medium, the refractive index of the surrounding is increased from 1 to 1.33. We firstly investigated the sensitivity of asymmetric Au NR-ND heterodimer to the surrounding medium. Figure 6(a) shows the scattering spectra of this heterodimer embedded in the medium with refractive index ($n = 1$). As the refractive index of this medium increases, both the FR and SPR modes of the scattering spectrum show about 100 nm and 60 nm red-shifts (see Fig. 6(a)). Since the dielectric screening effect caused by an embedded medium that reducing the energies of these modes [48]. The sensitivity of these modes to the local refractive index (RI) is given as the change in resonance mode per change in refractive index, and it is measured in nm per refractive index unit (RIU) [34]. The sensitivities for the FR and SPR modes are 303 nm/RIU and 182 nm/RIU, respectively. The calculated sensitivity values also indicate that when the surrounding medium is changed, the higher refractive index sensitivity of the Fano resonance [46]. Moreover, FR mode reveals promising applications in the field of the ultra-sensitive plasmonic sensor due to its high sensitivity [48].

Similarly, we investigated the sensitivity of asymmetric Au-Ag NR-ND heterodimer to the surrounding medium as shown in Fig. 6(b). The scattering spectra of this heterodimer embedded in the medium with refractive index($n = 1$), as shown in Fig. 6(b) black curve. As the refractive index of this medium around asymmetric heterodimer increases to 1.33, the Fano resonance and surface plasmon resonance modes (labeled as FR and SPR) are red-shifted about 112 nm and 96 nm. The sensitivities for the FR and SPR modes are 339 nm/RIU and 291 nm/RIU, respectively. The FR mode exhibits high sensitivity compared with SPR in the visible region. The same trend was observed in asymmetric Au-Ag heterodimers [65]. These results suggest that the FR mode with high sensitivity indicates that for most practical cases, it would be more convenient for optical sensing applications instead of the more commonly used SPR [65]. Thus, the proposed asymmetric heterodimers may find potential application in refractive index sensing.

Conclusions

In summary, theoretical studies of optical behaviors of morphologically asymmetric Au nanoring-nanodisk dimer, compositionally asymmetric Au-Ag nanoring dimer, and compositionally as well as geometrically asymmetric Au-Ag nanoring-nanodisk dimer have been performed by a rigorous computational approach. It has been found that as the inner radii of symmetrical Au NR dimer decreased the intensity of coupled bonding mode (mode I) and higher-order coupled bonding mode (mode II) drastically decreases and increases, respectively. The corresponding local-field and surface charge distribution profiles further clarify the spatial information of these modes. Also, we have shown that the aspect ratio is the predominant factor affecting the plasmon coupling behavior of symmetric Au NR dimer. Furthermore, we have demonstrated that the scattering spectrum of morphological asymmetric Au nanoring-nanodisk dimer and compositionally asymmetric Au-Ag nanoring dimer is expected to support the generation of a single Fano resonance due to reduced symmetry. The corresponding near-field and surface charge distribution profiles at this Fano resonance mode reveal that the interference of the dipole mode of ND and the quadrupole mode of NRs in morphologically asymmetric Au NR-ND dimer results in the Fano resonance. It is found that, in compositionally and geometrically asymmetric Au-Ag NR-ND heterodimers, double Fano resonances can be excited. The calculated corresponding local-field and surface charge distribution profiles provide a comprehensive understanding of the

generation of these resonance modes. Finally, at optimum asymmetric heterodimers, we discussed the effect of the refractive index on the Fano-type resonance. Our results suggest that the FR mode with high sensitivity indicates that for most practical cases, it would be more convenient for optical sensing applications instead of the more commonly used SPR. These findings provide the possibility to control optical response by using different asymmetric heterodimers consisting of different morphology and composition and the manifestation of higher-order Fano resonances, which have many potential applications such as in photonics and refractive index sensing.

Funding information This project was supported by National Natural Science Foundation of China (NSFC) (91850109, 61775021, 11474040); Education Department of Jilin Province (JJKH20181104KJ, JJKH20190555KJ); "111" Project of China (D17017); and Ministry of Education Key Laboratory for Cross-Scale Micro and Nano Manufacturing, Changchun University of Science and Technology.

References

1. Garcia MA (2011) Surface plasmons in metallic nanoparticles: fundamentals and applications. J Phys D Appl Phys 44:283001
2. Olson J, Dominguez-Medina S, Hoggard A, Wang L-Y, Chang W-S, Link S (2015) Optical characterization of single plasmonic nanoparticles. Chem Soc Rev 44:40–57
3. Noguez C (2007) Surface plasmons on metal nanoparticles: the influence of shape and physical environment. J Phys Chem C 111:3806–3819
4. Verma S, Rao BT, Detty AP, Ganesan V, Phase DM, Rai SK, Bose A, Joshi SC, Kukreja LM (2015) Surface plasmon resonances of Ag-Au alloy nanoparticle films grown by sequential pulsed laser deposition at different compositions and temperatures. J Appl Phys 117:133105
5. Pathak NK, Ji A, Sharma RP (2014) Tunable properties of surface plasmon resonances: the influence of core–shell thickness and dielectric environment. Plasmonics 9:651–657
6. Špačková B, Wrobel P, Bocková M, Homola J (2016) Optical biosensors based on plasmonic nanostructures: a review. Proc IEEE 104:2380–2408
7. Luk'yanchuk B, Zheludev NI, Maier SA, Halas NJ, Nordlander P, Giessen H, Chong CT (2010) The Fano resonance in plasmonic nanostructures and metamaterials. Nat Mater 9:707–715
8. Barnes WL, Dereux A, Ebbesen TW (2003) Surface plasmon subwavelength optics. Nature 424:824–830
9. Gallinet B, Martin OJF (2011) Influence of electromagnetic interactions on the line shape of plasmonic Fano resonances. ACS Nano 5:8999–9008
10. Zhang KJ, Da B, Ding ZJ (2018) Effect of asymmetric morphology on coupling surface plasmon modes and generalized plasmon ruler. Ultramicroscopy 185:55–64
11. Halas NJ, Lal S, Chang WS, Link S, Nordlander P (2011) Plasmons in strongly coupled metallic nanostructures. Chem Rev 111:3913–3961
12. Sheikholeslami S, Jun Y-W, Jain PK, Alivisatos AP (2010) Coupling of optical resonances in a compositionally asymmetric plasmonic nanoparticle dimer. Nano Lett 10:2655–2660
13. Roopak S, Kumar Pathak N, Sharma R, Ji A, Pathak H et al (2016) Numerical simulation of extinction spectra of plasmonically coupled nanospheres using discrete dipole approximation: influence of compositional asymmetry. Plasmonics 11:1603–1612
14. Nguyen TK, Le TD, Dang PT, Le KQ (2017) Asymmetrically engineered metallic nanodisk clusters for plasmonic Fano resonance generation. J Opt Soc Am B 34:668–672
15. Zong X, Li L, Liu Y (2019) Dark plasmon in asymmetric nanoring arrays on conducting substrates and related applications. Opt Mater Express 9:870–877
16. Schubert I, Sigle W, van Aken PA, Trautmann C, Toimil-Molares ME (2015) STEM-EELS analysis of multipole surface plasmon modes in symmetry-broken AuAg nanowire dimers. Nanoscale 7:4935–4941
17. Li Z, Cakmakyapan S, Butun B, Daskalaki C, Tzortzakis S, Yang X, Ozbay E (2014) Fano resonances in THz metamaterials composed of continuous metallic wires and split ring resonators. Opt Express 22:26572–26584
18. Chen F, Alemu N, Johnston RL (2011) Collective plasmon modes in a compositionally asymmetric nanoparticle dimer. AIP Adv 1:032134
19. Brown LV, Sobhani H, Lassiter JB, Nordlander P, Halas NJ (2010) Heterodimers: plasmonic properties of mismatched nanoparticle pairs. ACS Nano 4:819–832
20. Slaughter LS, Wu Y, Willingham BA, Nordlander P, Link S (2010) Effects of symmetry breaking and conductive contact on the plasmon coupling in gold nanorod dimers. ACS Nano 4:4657–4666
21. Huang C-P, Yin X-G, Kong L-B, Zhu Y-Y (2010) Interactions of nanorod particles in the strong coupling regime. J Phys Chem C 114:21123–21131
22. Encina ER, Coronado EA (2010) On the far field optical properties of Ag−Au nanosphere pairs. J Phys Chem C 114:16278–16284
23. Abdulla HM, Thomas R, Swathi RS (2018) Overwhelming analogies between plasmon hybridization theory and molecular orbital theory revealed: the story of plasmonic heterodimers. J Phys Chem C 122:7382–7388
24. Göeken K, Subramaniam V, Gill R (2015) Enhancing spectral shifts of plasmon-coupled noble metal nanoparticles for sensing applications. Phys Chem Chem Phys 17:422–427
25. Hao F, Nordlander P, Sonnefraud Y, Dorpe PV, Maier SA (2009) Tunability of subradiant dipolar and Fano-type plasmon resonances in metallic ring/disk cavities: implications for nanoscale optical sensing. ACS Nano 3:643–652
26. Sonnefraud Y, Verellen N, Sobhani H, Vandenbosch GAE, Moshchalkov VV, van Dorpe P, Nordlander P, Maier SA (2010) Experimental realization of subradiant, superradiant, and Fano resonances in ring/disk plasmonic nanocavities. ACS Nano 4:1664–1670
27. Fang Z, Cai J, Yan Z, Nordlander P, Halas NJ, Zhu X (2011) Removing a wedge from a metallic nanodisk reveals a Fano resonance. Nano Lett 11:4475–4479
28. Khan AD, Miano G (2014) Investigation of plasmonic resonances in mismatched gold nanocone dimers. Plasmonics 9:35–45
29. Wu D, Jiang S, Cheng Y, Liu X (2012) Fano-like resonance in symmetry-broken gold nanotube dimer. Opt Express 20:26559–26567
30. Qiu J, Xie M, Lyu Z, Gilroy KD, Liu H, Xia Y (2019) General approach to the synthesis of heterodimers of metal nanoparticles through site-selected protection and growth. Nano Lett 19:6703–6708
31. Bigelow NW, Vaschillo A, Camden JP, Masiello DJ (2013) Signatures of Fano interferences in the electron energy loss spectroscopy and cathodoluminescence of symmetry-broken nanorod dimers. ACS Nano 7:4511–4519

32. Tsai CY, Lin JW, Wu CY, Lin PT, Lu TW, Lee PT (2012) Plasmonic coupling in gold nanoring dimers: observation of coupled bonding mode. Nano Lett 12:1648–1654
33. Forcherio GT, Blake P, DeJarnette D, Roper DK (2014) Nanoring structure, spacing, and local dielectric sensitivity for plasmonic resonances in Fano resonant square lattices. Opt Express 22:17791–17803
34. Koya AN, Ji B, Hao Z, Lin J (2016) Controlling optical field enhancement of a nanoring dimer for plasmon-based applications. J Opt 18:055007
35. Devaraj V, Choi J, Kim C-S, Oh J-W, Hwang Y-H (2018) Numerical analysis of nanogap effects in metallic nano-disk and nano-sphere dimers: high near-field enhancement with large gap sizes. J Korean Phys Soc 72:599–603
36. Jain PK, El-Sayed MA (2010) Plasmonic coupling in noble metal nanostructures. Chem Phys Lett 487:153–164
37. Bordley JA, Hooshmand N, El-Sayed MA (2015) The coupling between gold or silver nanocubes in their homo-dimers: a new coupling mechanism at short separation distances. Nano Lett 15: 3391–3397
38. Hooshmand N, Mousavi HS, Panikkanvalappil SR, Adibi A, El-Sayed MA (2017) High-sensitivity molecular sensing using plasmonic nanocube chains in classical and quantum coupling regimes. Nano Today 17:14–22
39. Le KQ, Alù A, Bai J (2015) Multiple Fano interferences in a plasmonic metamolecule consisting of asymmetric metallic nanodimers. J Appl Phys 117:023118
40. Lassiter JB, Sobhani H, Knight MW, Mielczarek WS, Nordlander P, Halas NJ (2012) Designing and deconstructing the Fano lineshape in plasmonic nanoclusters. Nano Lett 12:1058–1062
41. Bachelier G, Russier-Antoine I, Benichou E, Jonin C, Del Fatti N et al (2008) Fano profiles induced by near-field coupling in heterogeneous dimers of gold and silver nanoparticles. Phys Rev Lett 101: 197401
42. Lombardi A, Grzelczak MP, Pertreux E, Crut A, Maioli P, Pastoriza-Santos I, Liz-Marzán LM, Vallée F, del Fatti N (2016) Fano interference in the optical absorption of an individual gold–silver nanodimer. Nano Lett 16:6311–6316
43. Teo SL, Lin VK, Marty R, Large N, Llado EA, Arbouet A, Girard C, Aizpurua J, Tripathy S, Mlayah A (2010) Gold nanoring trimers: a versatile structure for infrared sensing. Opt Express 18:22271–22282
44. Koya AN, Lin J (2016) Bonding and charge transfer plasmons of conductively bridged nanoparticles: the effects of junction conductance and nanoparticle morphology. J Appl Phys 120:093105
45. Prodan E, Radloff C, Halas NJ, Nordlander P (2003) A hybridization model for the plasmon response of complex nanostructures. Science 302:419–422
46. Niu L, Zhang JB, Fu YH, Kulkarni S, Anchuk B (2011) Fano resonance in dual-disk ring plasmonic nanostructures. Opt Express 19:22974–22981
47. Zhang X, Liu F, Yan X, Liang L (2020) Multipolar Fano resonances in concentric semi-disk ring cavities. Optik 200:163416
48. Ding Y, Liao Z (2015) Asymmetric split nanorings for Fano induced plasmonic sensor in visible region. Phys B Condens Matter 464:51–56
49. He J, Fan C, Wang J, Ding P, Cai G, Cheng Y, Zhu S, Liang E (2013) A giant localized field enhancement and high sensitivity in an asymmetric ring by exhibiting Fano resonance. J Opt 15:025007
50. Wu X, Dou C, Xu W, Zhang G, Tian R, Liu H (2019) Multiple Fano resonances in nanorod and nanoring hybrid nanostructures. Chin Phys B 28:014204
51. Johnson PB, Christy RW (1972) Optical constants of the noble metals. Phys Rev B 6:4370–4379
52. Palk ED (1985) Handbook of optical constants of solids, vol 3. Academic Press, p 804
53. Cui J, Ji B, Song X, Lin J (2019) Efficient modulation of multipolar Fano resonances in asymmetric ring-disk/split-ring-disk nanostructure. Plasmonics 14:41–52
54. Schmidt FP, Ditlbacher H, Hofer F, Krenn JR, Hohenester U (2014) Morphing a plasmonic nanodisk into a nanotriangle. Nano Lett 14: 4810–4815
55. Koya AN, Ji B, Hao Z, Lin J (2015) Resonance hybridization and near field properties of strongly coupled plasmonic ring dimer-rod nanosystem. J Appl Phys 118:113101
56. Kasani S, Zheng P, Wu N (2018) Tailoring optical properties of a large-area plasmonic gold nanoring array pattern. J Phys Chem C 122:13443–13449
57. Aizpurua J, Hanarp P, Sutherland DS, Käll M, Bryant GW, García de Abajo FJ (2003) Optical properties of gold nanorings. Phys Rev Lett 90:057401
58. Ye J, Van Dorpe P, Lagae L, Maes G, Borghs G (2009) Observation of plasmonic dipolar anti-bonding mode in silver nanoring structures. Nanotechnology 20:465203
59. Tsai C-Y, Chang K-H, Wu C-Y, Lee P-T (2013) The aspect ratio effect on plasmonic properties and biosensing of bonding mode in gold elliptical nanoring arrays. Opt Express 21:14090–14096
60. Wang W, Yu P, Zhong Z, Tong X, Liu T, Li Y, Ashalley E, Chen H, Wu J, Wang Z (2018) Size-dependent longitudinal plasmon resonance wavelength and extraordinary scattering properties of Au nanobipyramids. Nanotechnology 29:355402
61. Feng HY, Luo F, Meneses-Rodríguez D, Armelles G, Cebollada A (2015) From disk to ring: aspect ratio control of the magnetoplasmonic response in au/co/au nanostructures fabricated by hole-mask colloidal lithography. Appl Phys Lett 106:083105
62. Wang L, Liu Z, Yi X, Zhang Y, Li H, Li J, Wang G (2016) Analysis of symmetry breaking configurations in metal nanocavities: identification of resonances for generating high-order magnetic modes and multiple tunable magnetic-electric Fano resonances. J Appl Phys 119:173106
63. Li G, Hu H, Wu L (2019) Tailoring Fano lineshapes using plasmonic nanobars for highly sensitive sensing and directional emission. Phys Chem Chem Phys 21:252–259
64. Chahinez D, Reji T, Andreas R (2018) Modeling of the surface plasmon resonance tunability of silver/gold core–shell nanostructures. RSC Adv 8:19616–19626
65. Peña-Rodríguez O, Pal U, Campoy-Quiles M, Rodríguez-Fernández L, Garriga M, Alonso MI (2011) Enhanced Fano resonance in asymmetrical Au:Ag heterodimers. J Phys Chem C 115: 6410–6414